Journal of Magnetism and Magnetic Materials 533 (2021) 168015

Contents lists available at ScienceDirect

Journal of Magnetism and Magnetic Materials

journal homepage: www.elsevier.com/locate/jmmm

Research articles

The magnetic, electronic, optical, and structural properties of the AB_2O_4 (A = Mn, Fe, co; B = Al, Ga, In) spinels: Ab initio study

V.S. Zhandun

Kirensky Institute of Physics – Federal Research Center "Krasnoyarsk Science Centre, Siberian Branch of the Russian Academy of Sciences", 660036 Krasnoyarsk, Russia

ARTICLE INFO

Keywords:
Ab initio calculations
Spinel
Magnetic and electronic properties
Optical properties
Bandgap width

ABSTRACT

The effect of cation composition on the magnetic, electronic, optical, and structural properties of the spinel oxides AB_2O_4 (A = Fe, Mn, Co; B = Al, Ga, In) were studied within DFT-GGA + U approximation. The spinels were considered both in the normal and inverse structure. FeB_2O4 (B = Al, Ga, In) spinels have an inverse structure, whereas AB_2O_4 (A = Mn, Co; B = Al, Ga, In) prefer a normal structure. We find that the studied spinels are antiferromagnetic materials with the composition-dependent bandgap. The bandgap width is determined by the minimum of the conductive s-band formed by B-site cations states and can be increased by the applied pressure. The microscopic mechanisms of the relationship between composition, structural and electronic properties are analyzed. The ability to manipulate the structural, electronic, and optical properties is attributed to the different s-orbital energies and sizes of the B-site cations.

1. Introduction

The ability to control the magnetic, electronic, and optical properties of compounds and adjust the desired response of the system by changing the composition of the material is of undoubted importance for application areas, such as high-density magnetic recording, microwave devices, and magnetic fluids. The transition metal-containing spinels are a good candidate for this due to the huge variety of their properties in the dependence on the crystal structure as well as the chemical composition.

The spinels can be found in two structural modifications: normal and inverse spinel. The crystal structure of normal spinel has general configuration $A^{2+}B^{3+}{}_2O_4$, where bivalent A^{2+} and trivalent B^{3+} are tetrahedrally and octahedrally coordinated cations, respectively. An inverse spinel is an alternative arrangement where the A-site ions and half of the B-site ions switch places. Inverse spinels have the chemical formula $B^{3+}(A^{2+}B^{3+})O_4$, where the bivalent A^{2+} and half of the trivalent B ions occupy octahedral sites, and the other trivalent B ions are on tetrahedral sites.

In the present paper, we study how the properties of spinels depend on the cations on the A- and B-sites. This is useful for the subsequent targeted synthesis of compounds with specified controlled by the chemical composition properties. For this, we have performed ab initio calculation and comparison of the structural, magnetic, optical, and electronic properties of the spinel oxides AB_2O_4 (A = Mn, Fe, Co; B = Al, Ga, In) with the different cations on A^{2+}- and B^{3+}-sites. Some spinels from the series ($MnAl_2O_4$ [1–4], $CoAl_2O_4$ [5–9], $FeAl_2O_4$ [10–13], $CoGa_2O_4$ [14–17]) are well- studied materials, whereas other spinels ($MnGa_2O_4$ [18,19], $MnIn_2O_4$ [20–22], $FeGa_2O_4$ [23–25]) are still poorly understood or not studied yet ($FeIn_2O_4$, $CoIn_2O_4$). For example, unusual magnetic properties of MAl_2O_4 compounds are known since 1964. Despite this, the type of magnetic order at low temperatures is still unclear now. In [26] authors using susceptibility measurements and neutron powder diffraction study the magnetic ordering of $MnAl_2O_4$ and they have found a collinear antiferromagnetic ordering at the Neel temperature $T_N = 6$ K. The finding of the long-range magnetic order in $FeAl_2O_4$ was failed. However, neutron diffraction and Mössbauer experiments [27,28] indicated a spin-glass-like transition in $FeAl_2O_4$. In turn, for $CoAl_2O_4$ a long-range ordered magnetic state was observed below 4 K. The low-temperature magnetic behavior in $CoGa_2O_4$ reveals an antiferromagnetic order with $T_N = 10$ K [14]. In contrast to most spinels in which antiferromagnetic order is observed [4,8,12,14,18–20], $FeGa_2O_4$ is reported to be ferromagnetic [23]. At the same time, in [29] authors, based on the analysis of the scattering intensity, suggested that magnetic interactions of different sign coexist in the $FeGa_2O_4$ system. Another issue is associated with what type of structure will have a spinel with a certain composition. It is a common feature that the spinels have the partially inverse structure. The degree of inversion is related to the synthesis conditions but is also determined by the spinel composition. Thus, it seems that manganese and cobalt atoms tend to occupy tetrahedral positions [1–9,14–18] and hence, Mn- and Co-based spinels form

E-mail address: jvc@iph.krasn.ru.

https://doi.org/10.1016/j.jmmm.2021.168015
Received 15 September 2020; Received in revised form 7 April 2021; Accepted 8 April 2021
Available online 16 April 2021

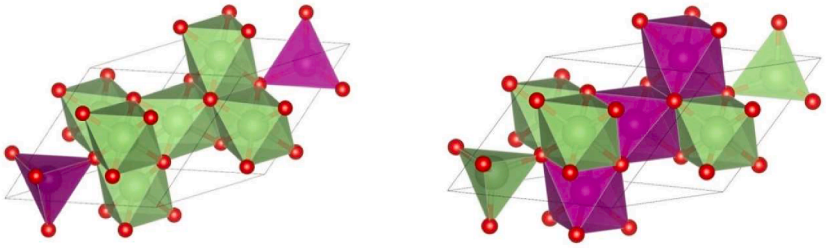

(a) (b)

Fig. 1. Crystal structure of normal (a) and inverse (b) spinels. The nearest environment of A^{2+} and B^{3+} ions are shown by purple and green color, respectively; oxygen atoms are shown by red balls.

a structure close to the normal. In contrast, the iron atoms seem to prefer octahedral sites [15,24,30] and hence, Fe-based spinels form a structure close to the inverse. Nevertheless, some studies report about the synthesis of $FeGa_2O_4$ spinel with the high percentage of iron atoms at the tetrahedral sites [23]. Therefore, the issues of the i) energetic advantage of the normal or inverse structure in spinels, depending on the composition, ii) magnetic ordering in the $FeGa_2O_4$ spinel still needs to be worked out, including by ab initio methods.

Despite many experimental and theoretical works devoted to AB_2O_4 spinels (A = Mn, Fe, Co; B = Al, Ga, In), there are no theoretical comparative studies of changes in the properties of spinels depending on the composition of the A- and B-sites in the literature. Therefore in the present paper, we study the dependence of the electronic, magnetic, and optical properties on the location and type of A- and B-site cations and analyze the microscopic origins of these dependencies.

The paper is organized as follows. In Sec. II, we give a short description of the computational details, in Sec. IIIA and IIIB, the comparison of magnetic, optic, and electronic properties of the normal and inverse spinels are reported. In the last Section, we make conclusions.

2. Calculation details

All ab initio calculations presented in this paper are performed using the Vienna ab initio simulation package (VASP) [31] with projector augmented wave (PAW) pseudopotentials [32]. The valence electron configurations $3d^74s^2$, $3d^64s^2$ and $3d^54s^2$ were taken for Co, Fe and Mn atoms, $3s^23p^1$, $3d^{10}4s^24p^1$ and $4d^{10}5s^25p^1$ for Al, Ga and In atoms and $2s^22p^4$ for O atoms. The calculations are based on the density-functional theory with the Perdew-Burke-Ernzerhoff (PBE) parameterization [33] of the exchange–correlation functional and the generalized gradient approximation (GGA). The plane-wave cutoff energy was 500 eV. The Brillouin-zone integration is performed on the 8 × 8 × 8 Monkhorst-Pack mesh of special points [34]. We have used the GGA + U scheme within Dudarev's approximation [35] with U = 3.5 eV, 4, and 4.5 eV for Mn, Fe, and Co atoms, correspondingly (following Ref. [36]).

3. Results and discussion

3.1. The structural and magnetic properties

We begin our comparative investigations with the study of the structural properties of the normal and inverse spinels. In the structure of the normal spinel (Fig. 1a and b), bivalent A-site cations are in the tetrahedral environment of oxygen atoms, and trivalent B-site cations are surrounded by six oxygen ions located at the vertices of the octahedron. In the inverse spinel structure (Fig. 1c and d), bivalent A-site cations are located in the center of half the octahedron formed by oxygen atoms, and trivalent B-site cations are located both in the centers of the other half of the octahedra and in the centers of the oxygen tetrahedra. As it follows from Refs. [1–22], the experimentally synthesized spinel oxides at room temperature have a cubic structure with an fcc unit cell (space group of symmetry Fd3 ¯m). However, it is known some spinels (for example $FeMn_2O4$ [37–38]) can be found in the tetragonal I4/amd phase. Therefore we checked this possibility also. It was obtained that the cubic structure is lower by energy for the Mn-based spinels, $FeAl_2O_4$, and $CoAl_2O_4$ spinels; in the other compounds ($FeGa_2O_4$, $FeIn_2O_4$, $CoGa_2O_4$ and $CoIn_2O_4$), the tetragonal phase has the lowest energy. Nevertheless, the experimental studies [15–16,23–24] unambiguously report the cubic Fd3 ¯m structure for $FeGa_2O_4$ and $CoGa_2O_4$ compounds, while the information about $FeIn_2O_4$, $CoIn_2O_4$ crystal structure is absent in the literature. Thus, based on existing experimental data, we chose the cubic structure as a reference structure for a qualitative comparison of composition-dependent spinel properties relative to each other. (Note that the properties of spinels in the cubic and tetragonal phases are qualitatively close to each other).

Table 1
The total energies (eV) of the ferromagnetic (FM) and antiferromagnetic (AFM) phases in the normal and inverse Fe-based spinels. The energy of the antiferromagnetic state is taken as zero.

	$FeAl_2O_4$	$FeGa_2O_4$	$FeIn_2O_4$
Normal spinel			
FM	0.118	−0.005	−0.012
AFM	0.000	0.000	0.000
Inverse spinel			
FM	0.630	0.012	0.023
AFM	0.000	0.000	0.000

Both ferromagnetic (FM) and antiferromagnetic (AFM) phases were checked as the ground state for all spinels. According to our calculations, Mn- and Co-based spinels has the AFM phase as the ground magnetic state, which agrees with the experimental results [4,8,12,14,18–20]. The AFM state also has the lowest energy in the inverse Fe-based spinels (Table 1). However, as seen from Table 1 in $FeGa_2O_4$ and $FeIn_2O_4$ spinels the AFM and FM phases are close by energy (especially in $FeGa_2O_4$ spinel) that can be evidence of the competition between exchange interactions in them. This is consistent with the conclusions of the Ref. [29], in which the authors reveal that magnetic interactions of different sign coexist in the $FeGa_2O_4$. Since we consider ideal normal (or inverse) structure, in real partially inverse spinels the ferromagnetic interactions can prevail over antiferromagnetic interactions regardless of the occupancy of the tetrahedral and octahedral positions. Note also, that in normal Fe-based $FeGa_2O_4$ and $FeIn_2O_4$ compounds the FM phase has a lower energy than AFM phase (Table 1). These can explain the experimental observation of ferromagnetic ordering in the $FeGa_2O_4$ spinel [23].

The geometry of all compounds was fully optimized. Calculated optimized lattice parameters, magnetic moments, and the total energies of the antiferromagnetic phases are shown in Tables 2–4. Our calculation showed that the structure of normal spinel (where A-cations are in the tetrahedral position) is lower by energy in compounds with A = Mn and Co (Tables 2–4). This agrees with the experimental results for the

Table 2
Lattice parameter (a), total energy (E), transition metal magnetic moment (μ), distances within tetrahedral (d_{tet}) and octahedral groups (d_{oct}) in normal and inverse MnB_2O_4 spinels.

	Normal spinel			Inverse spinel		
	Al	Ga	In	Al	Ga	In
a, Å	8.31	8.54	9.12	8.34	8.52	9.07
E, eV	−106.360	−92.326	−88.712	−101.835	−90.580	−86.491
μ, μ_B	4.57	4.58	4.60	4.56	4.58	4.61
d_{tet}, Å	2.02	2.04	2.11	2.01	2.02	2.08
d_{oct}, Å	1.94	2.03	2.20	1.89	2.03	2.19

Table 3
Lattice parameter (a), total energy (E), magnetic moment (μ), distances within tetrahedral (d_{tet}) and octahedral groups (d_{oct}) in normal and inverse FeB_2O_4 spinels.

	Normal spinel			Inverse spinel		
	Al	Ga	In	Al	Ga	In
a, Å	8.23	8.50	9.10	8.25	8.50	9.05
E, eV	−100.567	−85.421	−80.818	−101.152	−87.073	−82.330
μ, μ_B	3.72	3.75	3.80	3.71	3.75	3.77
d_{tet}, Å	2.00	2.02	2.07	2.01	2.03	2.06
d_{oct}, Å	1.80	2.03	2.22	1.91	2.03	2.21

Table 4
Lattice parameter (a), total energy (E), magnetic moment (μ), distances within tetrahedral (d_{tet}) and octahedral groups (d_{oct}) in normal and inverse CoB_2O_4 spinels.

	Normal spinel			Inverse spinel		
	Al	Ga	In	Al	Ga	In
a, Å	8.17	8.46	9.02	8.18	8.45	9.00
E, eV	−99.544	−86.272	−81.240	−98.601	−85.405	−80.112
μ, μ_B	2.71	2.73	2.75	2.71	2.74	2.76
d_{tet}, Å	1.97	2.00	2.04	2.00	2.01	2.03
d_{oct}, Å	1.93	2.03	2.21	1.96	2.02	2.20

known Mn- and Co-based spinels. In turn, in compounds with A = Fe, the structure of the inverse spinel, where A-site cations occupy an octahedral position, is most favorable by energy than the normal one (Table 3). Thus, iron atoms having a valence configuration with an even number of d-electrons prefer to have an octahedral environment. It should be noted that most spinels experimentally have partially inverse structures with composition-dependent degree of inversion. At that, the degree of inversion is different in different studies. Nevertheless, our results for the ideal normal/inverse spinels are well agreed with the experimental results. So, as followed from [18] the $MnGa_2O_4$ is partially inverse with 87% of the Mn atoms on tetrahedral A-sites. The experimental structure with high percentage of Mn atoms on tetrahedral sites is close to the ideal normal structure, obtained from our calculation. As for $FeGa_2O_4$, authors in [15] stated that it is a partially inverse spinel with 57% of Fe^{2+} ions on the tetrahedral site. Oles in [30] report about the synthesis of almost purely inverse spinel from neutron diffraction measurements. Based on these data, we can conclude that $FeGa_2O_4$ tends to form an inverse structure. This is consistent with our calculation, that is, a great tendency of an iron atom to occupy octahedral positions instead of tetrahedral ones, in contrast to manganese and cobalt atoms.

The transition metal magnetic moments increase slightly from B = Al to B = In. The analysis of the transition metal occupation numbers shows that the difference between Mn, Fe, and Co magnetic moments is related to the different occupations of the d-states by the d-electrons. The large values of the Mn magnetic moments appear due to the high-spin state of the Mn atom, where five d-electrons occupy spin-up d-states only. In Fe-based spinels, five d-electrons occupy spin-up states and the last electron is smeared between spin-down t2g-states (occupation numbers of these states are 0.33). In turn, in Co-based spinels, two of the d-electrons occupy spin-down eg-states (occupation numbers of these states are 0.98) leading to a reduction of the Co-magnetic moments.

The lattice parameters and the distances inside the tetrahedrons and octahedrons are shown in Tables 2–3 and Fig. 2. The lattice parameters and A-O and B-O bond lengths increase with the increase of the atomic number of B-site cations. However, the ratio of the distances inside

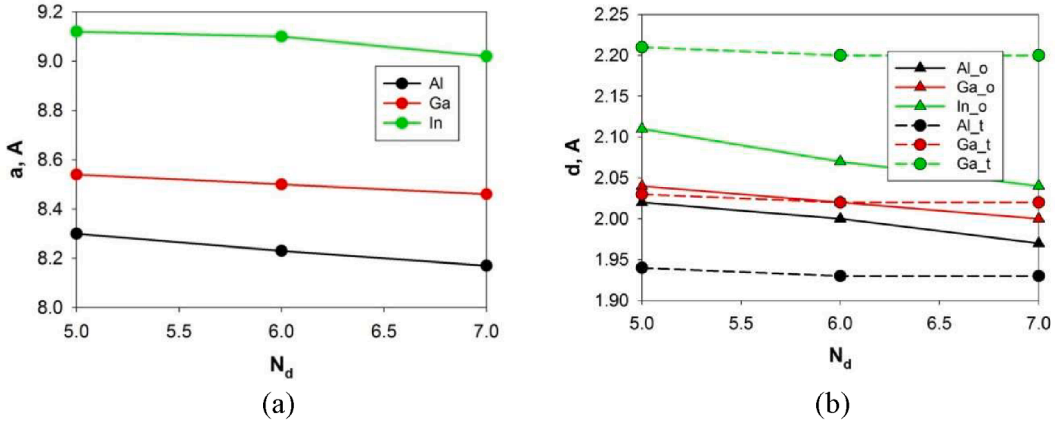

Fig. 2. Dependence of the lattice parameter (a) and interatomic distances inside tetrahedrons and octahedra (b) on the number of d-electrons of the transition metal atoms.

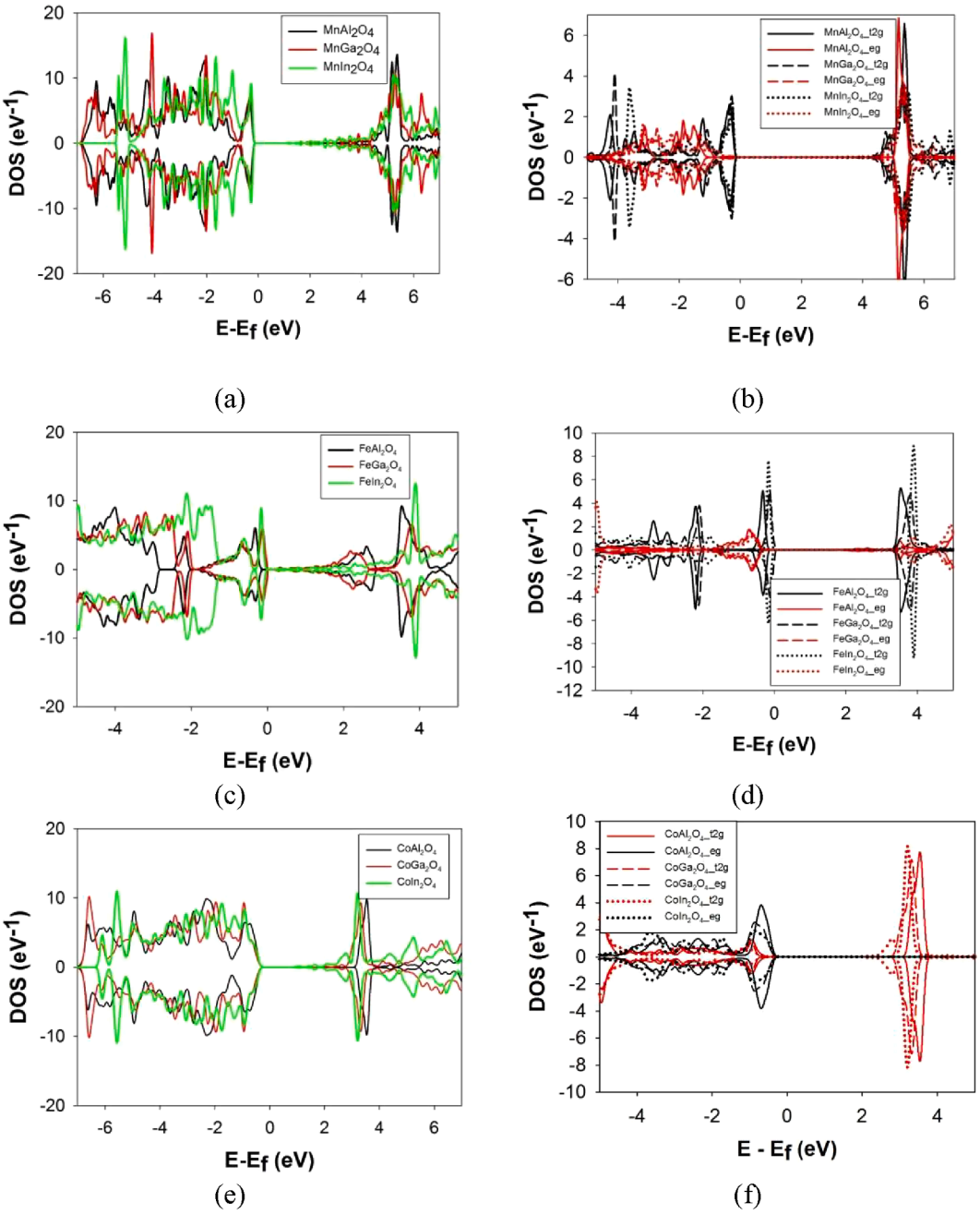

Fig. 3. The total (left) and partial (right) density of electronic states (DOS) of spinels MnB_2O_4 (a, b), FeB_2O_4 (c, d) CoB_2O_4 (e, f). Zero on the energy scale corresponds to the Fermi energy. Negative values of the density of states correspond to states with a negative spin.

tetrahedrons and octahedrons has non-trivial behavior. In AAl_2O_4 (A = Mn, Fe, Co) the distances inside the tetrahedrons are larger than the distances inside the octahedrons, indicating the large bond covalence within octahedrons. In compounds with B = Ga, the distances inside the tetrahedron the octahedrons are almost compared. However, in AIn_2O_4 (A = Mn, Fe, Co) the situation is inversed: the bond length within the tetrahedron becomes shorter than the bond length within the octahedron. This indicates the enhancement of covalence within the tetrahedron group. On the contrary, an increase in the atomic number of A -cation leads to a decrease in the lattice parameter and interatomic distances inside the tetrahedra and octahedra. Note also that the distances inside the octahedra grow faster with the increasing atomic number of the cation B than the distances inside the tetrahedra.

Table 5
The bandgap width (Eg) of the AB_2O_4 spinels.

	MnB_2O_4			FeB_2O_4			CoB_2O_4		
B-site cation	Al	Ga	In	Al	Ga	In	Al	Ga	In
Eg, eV	3.47	2.45	1.17	0.68	0.52	0.25	3.33	2.1	0.72

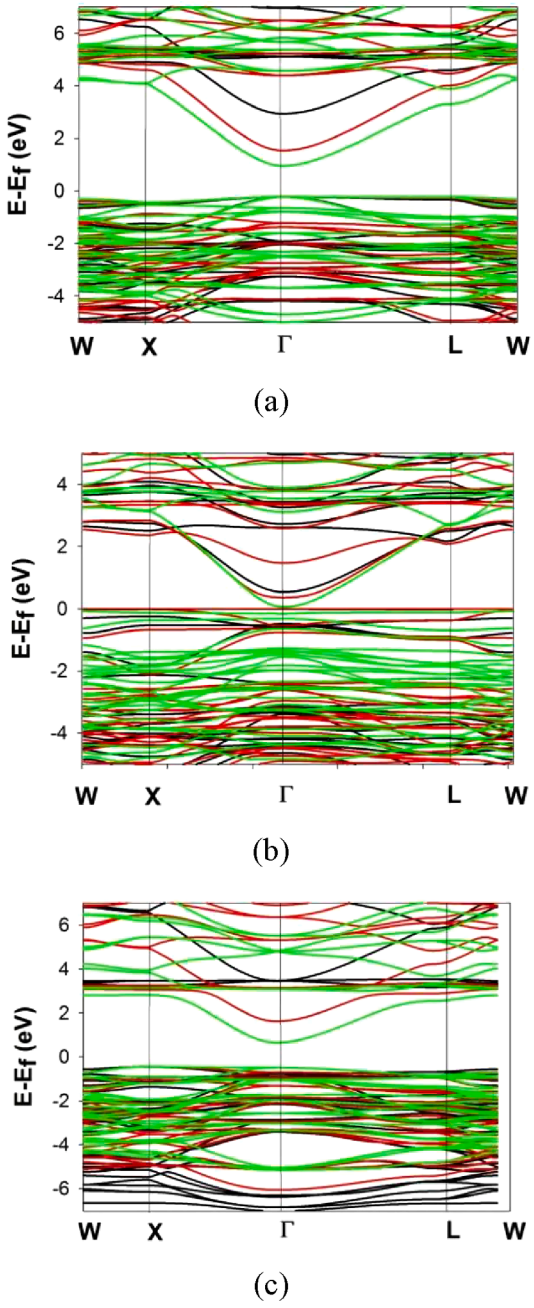

Fig. 4. The band structure of spinels MnB_2O4 (a), FeB_2O_4 (b) CoB_2O_4 (c). Zero on the energy scale corresponds to the Fermi energy.

3.2. Electronic and optical properties

The total density of electronic states and the partial density of d states with contributions to contributions by t2g- and eg-orbitals are shown in Fig. 3. All compounds have an energy gap that varies widely in the dependence on the cations at A- and B-sites (see Table 5). The largest bandgap is observed in spinels with B = Al, and the smallest bandgap width in compounds with indium, that is, an increase in the atomic number of B-site cations, leads to a decrease in the energy gap. This is because, as the atomic number of B-site cation increases, the lattice parameter and interatomic distance will be reduced. As a consequence binding forces between the valence electrons and the parent atoms will increase. Since the valence electrons are bound, more energy is required to make them free in the conduction band, causing the conduction band to move down, thus reducing the bandgap. So, a direct consequence of

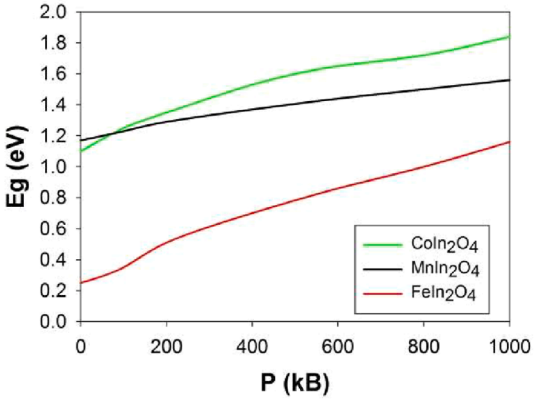

Fig. 5. The pressure dependence of the bandgap width in the AIn_2O_4 spinels.

decreasing the lattice constant is the increase in the energy gap. A similar, but less pronounced tendency toward an increase in the width of the energy gap is also observed with an increase in the number of d electrons on the A-site cation.

As seen in Fig. 3, well-localized t2g-electrons of transition metal formed the states near the Fermi energy, whereas more delocalized eg-states are located deeper in energy. The d-states of transition metals have strong hybridization with highly delocalized p-electrons of B-site cation and oxygen atoms in the wide energy range of [−6;−1] eV. The empty localized d-states of transition metals are high in energy ~5 eV in manganese spinels, ~4 eV in iron spinels, and ~4 eV in cobalt spinels. Thus, the bandgap mainly decreases due to the empty delocalized s- and p-states of B-site cations, which are forming conductive bands in the energy range near the Fermi energy.

An analysis of the band structure of spinels (Fig. 4) showed that for all spinels, the qualitative behavior of the bands practically the same. The lowest empty band, consisting of the s-states of B-site cation, has pronounced dispersion dependence, greatly narrowing the bandgap in the XΓ and LΓ directions. As seen, the decrease of the bandgap width is mainly related to the increase of the curvature of the conductive s-band and with its lowering down to the Fermi energy with the increase of the atomic number of B-site cation. The drop of the s-band is much faster than that of the transition metal d-states, due to the stronger delocalization of s-states. Therefore the conductive s-band has much more dispersion than the conduction band derived from empty d-states. The minimum of the conduction band is at point Γ. The highest energy valence band formed by the localized d-electrons of the A-site cations is almost flat in the entire phase space.

Since an increase in the atomic number of B-site cation leads to an increase in the lattice parameter and a decrease in the bandgap width, we examined how pressure will affect the bandgap width. Fig. 5 shows the dependence of the energy bandgap in AIn_2O_4 (A = Mn, Fe, Co) spinels, which have the smallest bandgap in a row (Al, Ga, In), on the applied hydrostatic pressure. Pressure leads to a decrease in the curvature of the conducting s-band due to a decrease in interatomic distances and lattice parameters. This, in turn, leads to the s states-based minimum of conduction band gets further from the Fermi energy level and, thus, the bandgap increases. The greatest increase is observed in $FeIn_2O_4$: at zero pressure it has the smallest bandgap among AIn_2O_4 spinels, however at the pressure P = 1000 kB the bandgap increases 5 times. The lowest growth of bandgap width is observed in the $MnIn_2O_4$ spinel: the growth of the bandgap width is 16%.

The optical absorption spectra are given in Fig. 6. The common tendency is the broadening of the absorption band with the increase of the atomic number of B-site cation. All spectra have a sharp peak at the low wavelength range of about 100–150 nm. This peak is related to the interband transitions from the low-lying wide p- and d- bands to the conductive bands. The increase of the atomic number of B-site cations

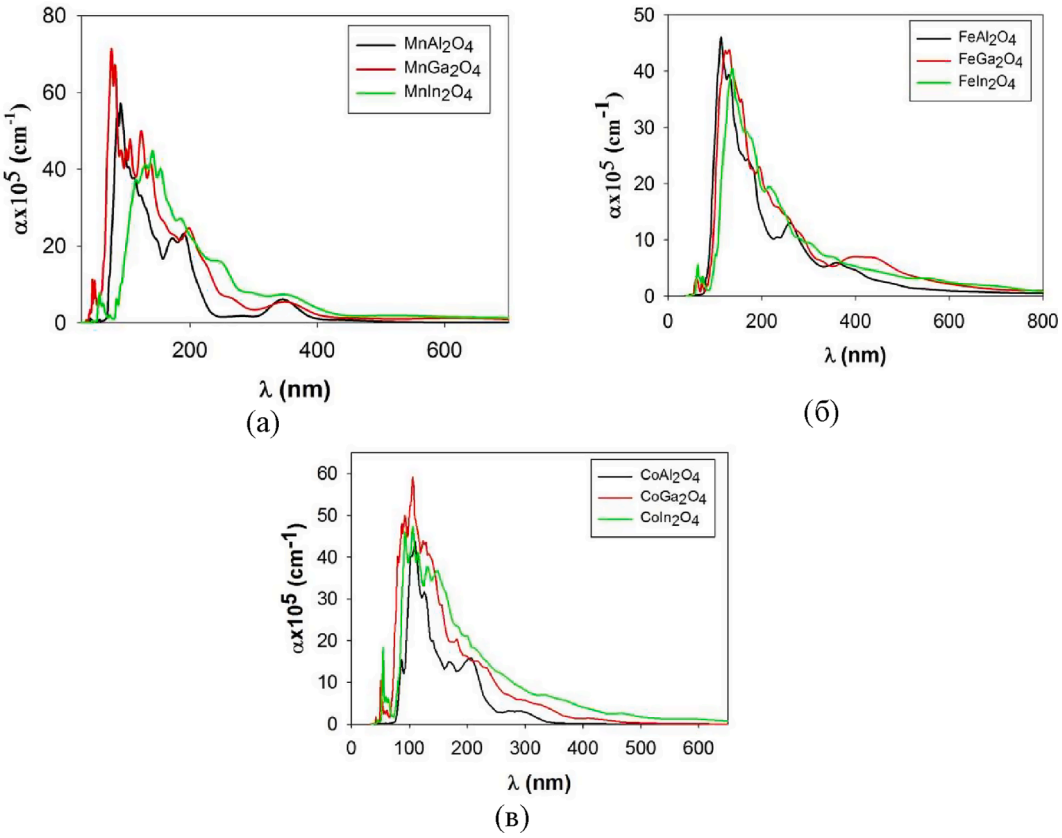

Fig. 6. The optical absorption spectra of MnX_2O4 (a), FeB_2O_4 (б) CoB_2O_4 (в) spinels.

shifts the peak to longer wavelengths. Notice that there are some small peaks at 200–270 eV and 300–400 eV. The latter peak is related to the transition from high-lying d-states of transition metal atoms to the s-bands formed by B-site cations states. The absorption bandwidth also slightly increases with the increase of the atomic number of B-site cations due to the s-band become closer to the Fermi energy level in the compounds with a large atomic number of B-site cations.

4. Conclusions

In conclusion, we have performed the calculation, comparison, and analysis of the structural, magnetic, electronic, and optical properties of the spinels AB_2O_4 (A = Mn, Fe, Co; B = Al, Ga, In). The lowest energy structure depends on the A-site cation: Fe-based compounds prefer inverse structure, whereas Mn- and Co-based spinels have a normal structure. All compounds show antiferromagnetic ordering and the presence of an energy bandgap. Increase in the atomic number of B-site cation results in the increase of lattice parameter and interatomic distances which in turn leads to the decrease of the bandgap width. The bandgap width mainly determined by the s-states of B-cations: the behavior of their s-band in the Brillouin zone has pronounced dispersion dependence due to the strong delocalization of s-states. This means that, with increasing of atomic number of B-site cation, the minimum of s-states conduction band come closer to the Fermi energy level and thus reduce the band gap. The applied hydrostatic pressure reduces the curvature of s-band and shifts the minimum of the s-band from the Fermi energy, thereby increasing the bandgap width. The absorption spectra reflect the difference in electronic properties and can be tuned by the varying of the composition or by the pressure. The calculated bandgaps as a function of composition provide a detailed practical guide to the synthesis of transition metal-based spinel oxides with the structural, magnetic, electronic, and optical properties required to achieve high efficiency in spintronics and optoelectronics.

CRediT authorship contribution statement

V.S. Zhandun: Conceptualization, Methodology, Validation, Software, Investigation, Writing - original draft.

Declaration of Competing Interest

The authors declare that they have no known competing financial interests or personal relationships that could have appeared to influence the work reported in this paper.

Acknowledgments

The reported study was funded by Russian Foundation for Basic Research, Government of Krasnoyarsk Territory, Krasnoyarsk Regional Fund of Science to the research project № 19-42-240016: «Control of structural, magnetic, electronic, and optical properties by pressure and intercalation into functional compounds with a spinel structure containing 3d and 4f ions» The calculations were performed with the computer resources of "Complex modeling and data processing research installations of mega-class" SRC "Kurchatovsky Institute" (http://ckp.urcki.ru).

Data availability

The data that support the findings of this study are available from the corresponding author upon reasonable request.

References

[1] S. Wanga, X. Wei, H. Gao, Y. Wei, Optik – Int. J. Light Electron Opt. 185 (2019) 301–310.
[2] R.C.S. Navarro, R.R. de Avillez, T.F. Goes, A.M.S. Gomes, J. Mater. Res. Technol. 9 (2020) 4194–4205.

[3] N. Tristan, J. Hemberger, A. Krimmel, H-A. Krug von Nidda, V. Tsurkan, A. Loidl. Phys. Rev. B 72 (2005) 174404-1–174404-9.
[4] S. Akbudaka, A.K. Kushwah, G. Uğurc, Ş. Uğurc, H. Yaşar Ocak, Ceram. Int. 44 (2018) 310–316.
[5] A. Nakatsuka, Y. Ikeda, Y. Yamasaki, N. Nakayama, T. Mizota, Solid State Commun. 128 (2003) 85–90.
[6] X. Duana, M. Pan, F. Yu, D. Yuan, J. Alloys Compd. 509 (2011) 1079–1083.
[7] F. Tielens, M. Calatayud, R. Franco, J.M. Recio, J. Perez-Ramırez, C. Minot, J. Phys. Chem. B 110 (2006) 988–995.
[8] T Suzuki, H Nagai, M Nohara, H Takagi. J. Phys.: Condens. Matter 19 (2007) 145265-1–145265-5.
[9] A. Walsh, S.-H. Wei, Y. Yan, M. M. Al-Jassim, J. A. Turner, M. Woodhouse, B. A. Parkinson. Phys. Rev. B 76 (2007) 165119-1–165119-9.
[10] F. Mukhtar, Z.N. Kayani, S. Riaz, S. Naseem, Ceram. Int. 44 (2018) 9550–9560.
[11] D.P. Dutta, G. Sharma, Mater. Sci. Eng. B 176 (2011) 177–180.
[12] J. Fukushima, Y. Hayashi, H. Takizawa, J. Asian Ceram. Soc. 1 (2013) 41–45.
[13] C.M. Yagnik, H.B. Mathur, Phys. C (Proc. Phys. Soc.) 1 (1968) 469–472.
[14] D. Fiorani, S. Viticoli, Solid State Commun. 25 (1978) 155–157.
[15] F. Leccabue, C. Pelosi, E. Agostinelli, V. Fares, D. Fiorani, E. Paparazzo, J. Cryst. Growth 79 (1986) 410–416.
[16] J.L. Soubeyroux, D. Fiorani, E. Agostinelli, J. Magnet. Magnet. Mater. 54–57 (1986) 83–84.
[17] Z. Xu, S. Yan, Z. Shi, Y. Yao, P. Zhou, H. Wang, Z. Zou, ACS Appl. Mater. Interfaces 8 (2016) 12887–12893.
[18] B. Boucher, A.G. Herpin, A. Oles, J. Appl. Phys. 37 (1966) 960–961.
[19] J.Y. Lee, D.S. Kim, C.W. Na, J. Park. J. Phys. Chem. C 111 (2007) 12207-12212.
[20] M.J. Martinez-Lope, M. Retuerto C. delaCalle, F. Porcher, J.A. Alonso. J. Solid State Chem. 187 (2012)172–176.
[21] M.F. Bekheet, L. Dubrovinsky, A. Gurlo, J. Solid State Chem. 230 (2015) 301–308.
[22] M.F. Bekheet, G. Miehe, C. Fasel, A. Gurlo, R. Riedel, Dalton Trans. 41 (2012) 3374–3376.
[23] I.S. Lyubutin, S.S. Starchikov, N.E. Gervits, C.-R. Lin, Y.-T. Tseng, K.-Y. Shih, J.-S. Lee, Yu.L. Ogarkova, A.O. Baskakov, K.V. Frolov, J. Phys. Chem. C 120 (2016) 25596–25603.
[24] J. Ghose, G.C. Hallam, D.A. Read, J. Phys. C: Solid State Phys. 10 (1977) 1051–1057.
[25] F. Leccabue, R. Panizzieri, B.E. Watts, D. Fiorani, E. Agostinelli, A. Testa, E. Paparazzo, J. Cryst. Growth 112 (1991) 644–650.
[26] W.L. Roth, J. Phys. Paris 25 (1964) 507–515.
[27] J.L. Soubeyroux, D. Fiorani, E. Agostinelli, S.C. Bhargava, J.L. Dormann. J. Phys. Paris 49, Suppl. 12 (1988) C8-1117–C8-1118.
[28] J.L. Dormann, M. Seqqat, D. Fiorani, M. Nogues, J.L. Soubeyroux, S.C. Bhargava, P. Renaudin, Hyperfine Interact. 54 (1990) 503–507.
[29] A. Wiedemann, P. Burlet, H. Schuerer, P. Convert, Solid State Commun. 38 (1981) 129–133.
[30] A. Oles, Acta Phys. Polonica 30 (1966) 125–134.
[31] G. Kresse, J. Furthmüller. Phys. Rev. B 54 (1996) 11169–11186.
[32] P. E. Blochl. Phys. Rev. B 50 (1994) 17953 - 17979; G. Kresse and D. Joubert. Phys. Rev. B. 59 (1999) 1758 - 1775.
[33] J.P. Perdew, K. Burke, M. Ernzerhof, Phys. Rev. Lett. 77 (1996) 3865–3868.
[34] H.J. Monkhorst, J.D. Pack, Phys. Rev. B 13 (1976) 5188–5192.
[35] S.L. Dudarev, G.A. Botton, S.Y. Savrasov, C.J. Humphreys, A.P. Sutton, Phys. Rev. B 57 (1998) 1505–1509.
[36] E. Sasıoglu, C. Friedrich, S. Blügel. Phys. Rev. B 83 (2011) 121101(R)-1 - 121101 (R)-4.
[37] R. Nepal, Q. Zhang, S. Dai, W. Tian, S.E. Nagler, R. Jin, Phys. Rev. B 97 (2018), 024410-1 - 024410-7.
[38] V.A.M. Brabers, Phys. Stat. Sol. 33 (1969) 563–572.